

Copper Hydroxide Nanoneedle and Nanotube Arrays Fabricated by Anodization of Copper

Xufeng Wu, Hua Bai, Jiaxin Zhang, Feng'en Chen, and Gaoquan Shi*

Department of Chemistry and Bio-organic Phosphorous Laboratory, Tsinghua University, Beijing 100084, People's Republic of China

Received: August 4, 2005; In Final Form: September 18, 2005

$\text{Cu}(\text{OH})_2$ nanoneedle and nanotube arrays were electrochemically synthesized by anodization of a copper foil in an aqueous solution of KOH. The nanoneedles and nanotubes were constructed from nanosheets of $\text{Cu}(\text{OH})_2$. Controlling the electrochemical conditions can qualitatively modulate the lengths, amounts, and shapes of $\text{Cu}(\text{OH})_2$ nanostructures. The composition of as-prepared $\text{Cu}(\text{OH})_2$ nanostructures has been confirmed by X-ray diffraction and select-area electron diffraction. The influences of the KOH concentration of the aqueous electrolyte, the reaction temperature, and current density on the morphology of $\text{Cu}(\text{OH})_2$ nanostructures were investigated, and the formation mechanism of the nanostructures is discussed. Furthermore, $\text{Cu}(\text{OH})_2$ nanoneedles can be successfully transformed to CuO nanoneedles with little morphology change by heating. This work developed a simple, clean, and effective route for fabrication of large area $\text{Cu}(\text{OH})_2$ or CuO nanostructured films.

Introduction

One-dimensional (1D) nanostructures (e.g., nanowire, nanotube, nanoribbon) have attracted a great deal of attention, mainly due to their unique electronic, magnetic, mechanical, or chemical properties.¹ Many techniques including template-guide growth,^{2,3} vapor–liquid–solid (VLS) synthesis,^{4,5} epitaxial electrodeposition,⁶ and chemical vapor deposition^{7,8} have been developed to synthesize these materials. However, the size and morphology control of 1D nanomaterials is still one of the challenging issues, because the control of nucleation and growth processes of nanostructures is rather difficult.

Basic Cu(II) salts and $\text{Cu}(\text{OH})_2$ with an orthorhombic structure have been studied extensively in the past several years. Matijević and co-workers investigated the relationship between the morphologies of homogeneously precipitated $\text{Cu}(\text{OH})_2$ and the solution compositions.^{9–11} Polycrystalline $\text{Cu}(\text{OH})_2$ nanowires and nanoribbons were synthesized through a two-step wet chemical route^{12,13} or by the interaction between a copper complex and NaOH at the aqueous–organic interface¹⁴ or prepared in aqueous solution of ammonia using Cu_2S nanowires as precursors.¹⁵ Single-crystalline $\text{Cu}(\text{OH})_2$ nanoribbon and nanotubes were successfully synthesized by surface oxidation of copper foil in alkaline solutions^{16,17} or anion exchange reaction using NaOH solution.¹⁸ However, control of the size, yield, and shape of the final nanomaterials has not yet been achieved.

It is well-known that electrochemical reaction can be accurately modulated by integrated charge passed through the electrochemical cell, and so the size and yield of the product may be easily controlled to some extent.^{19,20} Extensive work has been reported on the synthesis of 1D nanostructures through template-guided electrochemical deposition.^{21,22} Here, we report that $\text{Cu}(\text{OH})_2$ nanoneedles and scroll-like nanotube film can be simply grown by direct anodization of copper in an aqueous solution of KOH. To the best of our knowledge, this is the first

attempt to synthesize 1D inorganic nanostructures using an electrochemical method without any template and additives. In addition, CuO is a p-type semiconductor with a narrow band gap (1.2 eV). CuO-based materials have been used as high-temperature superconductors, catalysts, anode electrodes for batteries, and optical switches.^{23–26} In this work, we also report that CuO nanoneedle arrays can be easily generated by heating the $\text{Cu}(\text{OH})_2$ precursors in the temperature range 150–200 °C without obvious morphological changes.

Experimental Section

Typically, the growth of $\text{Cu}(\text{OH})_2$ nanoneedles and scroll-like nanotubes was carried out at room temperature in a one-compartment cell by the use of a model 263 potentiostat-galvanostat (EG&G Princeton Applied Research) under computer control. A copper foil (99.9%, Shanghai Chemical Reagent Co. Ltd., Shanghai, China) was used as the working electrode (surface area = 1.5 cm²). The counter electrode was a stainless steel sheet (AISI 304, surface area = 1.6 cm²). The typical electrolyte was an aqueous solution of KOH (≥84%; Beijing Fine Chemical Co. Ltd., Beijing, China). The solutions were deaerated by a dry nitrogen stream and maintained at a light overpressure during the experiments. $\text{Cu}(\text{OH})_2$ films were electrochemically grown at a constant current density of 1.5 mA cm⁻² in KOH aqueous solution with integrated charge control. The electrochemical deposition conditions are summarized in Table 1. After reaction, a faint-blue film was formed on the copper foil surface. Then the copper foil with the product was taken out from the solution and washed with distilled water and dried under vacuum at room temperature before characterizations. For the preparation of CuO nanoneedles, the $\text{Cu}(\text{OH})_2$ nanoneedle sample was heated to 150 °C for 3 h to complete dehydration, then the temperature was evaluated to 200 °C and kept for another 3 h to promote crystallization under nitrogen protection. Finally, the sample was naturally cooled to room temperature.

Scanning electron micrographs (SEMs) were taken by the use of a FEI Sirion 200 scanning electron microscope. X-ray

* To whom correspondence should be addressed. Phone: 86-10-62773743. Fax: 86-10-62771149. E-mail: gshi@tsinghua.edu.cn.

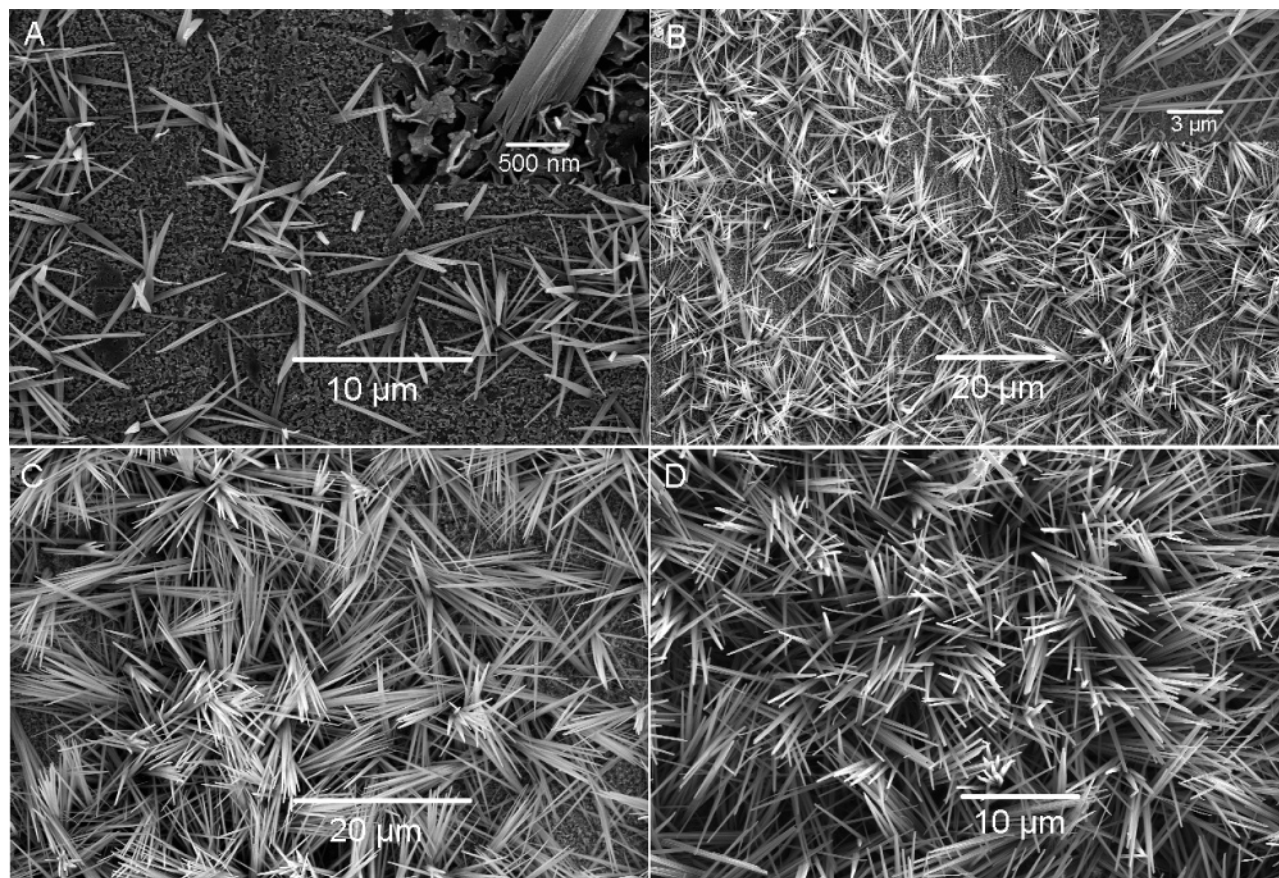


Figure 1. SEM images of as-prepared $\text{Cu}(\text{OH})_2$ nanoneedles deposited at a constant current density of 1.5 mA cm^{-2} in 2.0 mol L^{-1} KOH solution for different deposition times: (A) 300 s; (B) 500 s, insert contains a magnified view; (C) 1000 s; (D) 1500 s. $T = 28 \pm 2 \text{ }^\circ\text{C}$.

TABLE 1: The Products Formed by Anodization of a Copper Foil at a Constant Current Density of 1.5 mA cm^{-2} in the Media with Different Concentrations of KOH (C_{KOH}) and at Different Temperatures (T)

T ($^\circ\text{C}$)	C_{KOH} , 2 mol/L	C_{KOH} , 2.5 mol/L	C_{KOH} , 3 mol/L	C_{KOH} , 3.5 mol/L
2 ± 2	$\text{Cu}(\text{OH})_2$ nanoneedles	$\text{Cu}(\text{OH})_2$ nanoneedles	$\text{Cu}(\text{OH})_2$ nanoneedles	$\text{Cu}(\text{OH})_2$ nanoneedles
15 ± 2	$\text{Cu}(\text{OH})_2$ nanoneedles	$\text{Cu}(\text{OH})_2$ nanoneedles	$\text{Cu}(\text{OH})_2$ nanotubes	$\text{Cu}(\text{OH})_2$ nanotubes
28 ± 2	$\text{Cu}(\text{OH})_2$ nanoneedles	$\text{Cu}(\text{OH})_2$ nanotubes	$\text{Cu}(\text{OH})_2$ nanotubes	CuO nanoparticles

diffraction (XRD) was carried out by using an X-ray diffractometer model D8 advance (Bruker) with $\text{Cu K}\alpha$ radiation ($\lambda = 1.5418 \text{ \AA}$). Transmission electron micrographs (TEMs) and high-resolution TEMs were taken on a JEM 2010 (200 kV) transmission electron microscope (JEOL).

Results and Discussion

Figure 1 shows the typical SEMs of as-prepared $\text{Cu}(\text{OH})_2$ nanoneedle film formed by anodization a copper foil in 2.0 mol L^{-1} KOH solution at a constant current density of 1.5 mA cm^{-2} for different times. We can find that the amount of integrated charge passed through the cell during electrolysis process has influences on the length and the amount of $\text{Cu}(\text{OH})_2$ nanoneedles. When the deposition time was less than 150 s, no needle was observed on the copper surface. As the electrolysis time was increased to 300 s, the $\text{Cu}(\text{OH})_2$ pinelike needles with average length of $\sim 5 \mu\text{m}$ were grown sparsely on the copper surface (Figure 1A). The inset of Figure 1A demonstrates that the nanoneedle was composed of tightly arranged nanoribbons. Figure 1B and its insert image also clearly show the formation of $\text{Cu}(\text{OH})_2$ nanoneedles. Furthermore, as can be seen from parts B–D of Figure 1, when the electrolysis time increased from 300 to 1500 s, the length of the needles increased from ~ 5 to $\sim 15 \mu\text{m}$ and their amount was also markedly increased. Finally, pine-needle-like $\text{Cu}(\text{OH})_2$ covered the whole surface of the

copper substrate uniformly and compactly (Figure 1D). The nanoneedles are 500–550 nm in diameter at their roots and 100–120 nm at their sharp tips.

The formation of crystalline $\text{Cu}(\text{OH})_2$ was confirmed by the use of wide-angle X-ray diffraction. Figure 2A is the XRD pattern of an as-prepared $\text{Cu}(\text{OH})_2$ nanoneedle film covered copper foil. The indexed diffraction peaks except those marked with stars (they are attributed to the copper substrate) can be indexed to the orthorhombic phase of $\text{Cu}(\text{OH})_2$.²⁷ The diffraction lines are in good agreement with the corresponding literature values: $a = 2.949 \text{ \AA}$, $b = 10.59 \text{ \AA}$, $c = 5.256 \text{ \AA}$ (JCPDS 13-420). In comparison to those of the powder XRD pattern, the intensities of (111) and (130) lines are significantly enhanced, indicating that the crystalline $\text{Cu}(\text{OH})_2$ nanoneedles are on average roughly perpendicular to the copper substrate with a wide distribution of tilts.¹⁶ The weak diffraction peaks at 29.6, 42.3, and 61.4 can be assigned to cubic cuprous oxide (110), (200), and (220) planes (JCPDS 78-2076), which is a product of the side reaction



The structure of the nanoneedles was further investigated by TEM. As shown in Figure 2B, a nanoneedle is composed of layered nanoribbons. The widths of the ribbons are in the range

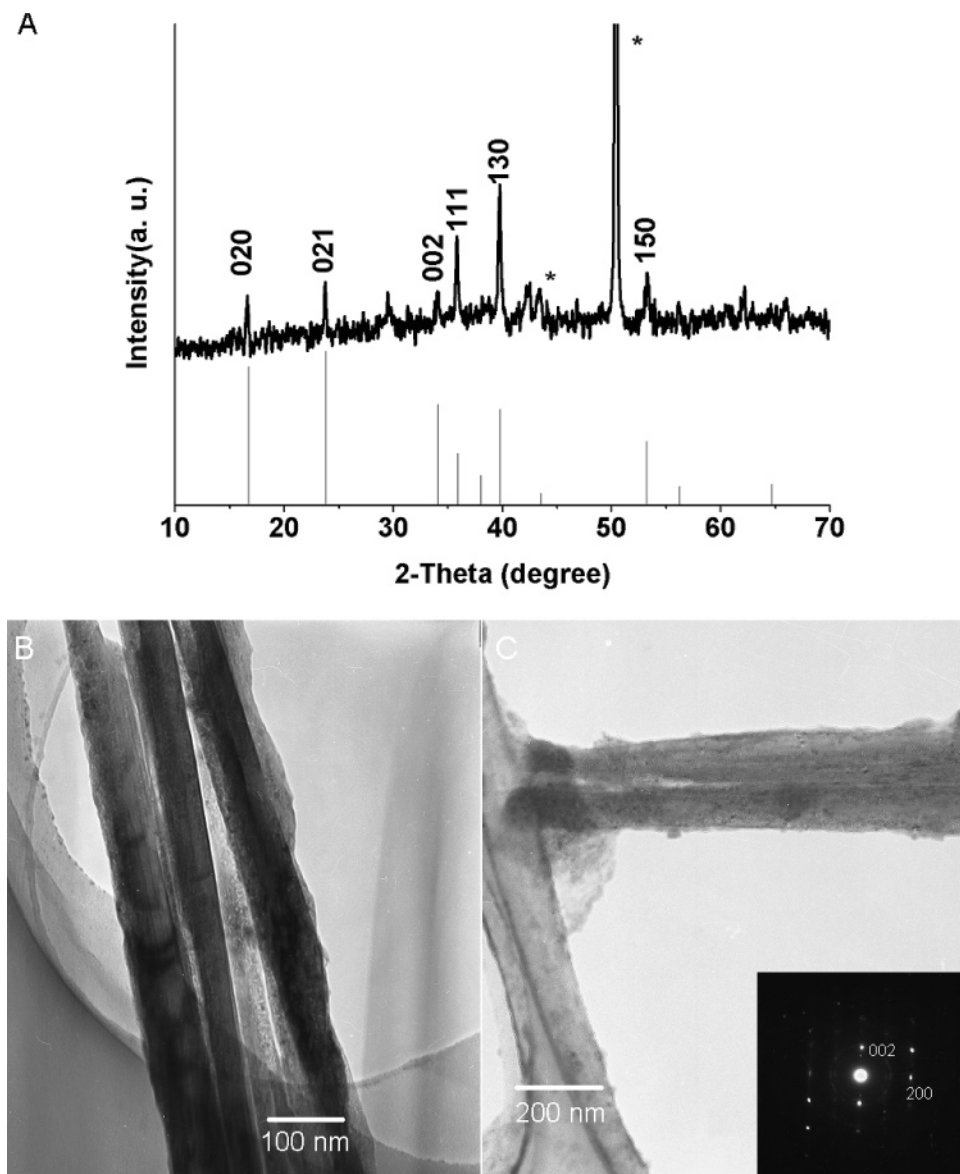


Figure 2. Typical XRD pattern and TEM images of as-prepared $\text{Cu}(\text{OH})_2$ nanoneedles deposited at a constant current density of 1.5 mA cm^{-2} in 2.0 mol L^{-1} KOH solution for 2.25 C cm^{-2} on a copper foil surface at 28°C : (A) XRD pattern; (B, C) TEM images (insert, SAED).

of 80–100 nm (Figure 2B–C). These can be confirmed further by the image inserted in Figure 1A. The selected area electron diffraction (SAED) pattern of a 100 nm wide ribbon (inset of Figure 2C) indicates that the ribbon is a single crystal. According to the diffraction patterns, $\text{Cu}(\text{OH})_2$ ribbons are arranged parallel to their (010) planes, and the preferential growth direction of the single-crystal nanoribbons is their [100] direction. Since $\text{Cu}(\text{OH})_2$ had been transformed to CuO nanocrystallites rapidly under the irradiation of a high-energy electron beam, we failed to get a high-resolution transmission electron microscope (HR-TEM) image of the $\text{Cu}(\text{OH})_2$ nanoribbon. Figure S1 shows a TEM image of the root part of a nanoribbon (A) and a HR-TEM image of a whole nanoribbon (B). According to Figure S1-B, $\text{Cu}(\text{OH})_2$ was transformed to CuO nanocrystallites by the irradiation of a high-energy electron beam. This also was confirmed by the SAED pattern shown as an inset of Figure S1-A.

As the other experimental parameters were kept unchanged, the morphology of $\text{Cu}(\text{OH})_2$ nanostructures depends strongly on the concentration of KOH (C_{KOH}). In the system described

above, when C_{KOH} was increased to over 2.5 mol L^{-1} , it was interesting to find that the nanoneedles were disappeared and scroll-like $\text{Cu}(\text{OH})_2$ nanotubes were formed on the copper foil. Figure 3 shows the typical SEM images of as-prepared $\text{Cu}(\text{OH})_2$ nanotube film formed by electrolysis of a copper foil in a 3 mol L^{-1} KOH aqueous solution at 1.5 mA cm^{-2} for 2.7 C cm^{-2} at 28°C . The low-magnified SEM image of the nanotubes is similar to that of as-prepared $\text{Cu}(\text{OH})_2$ nanoneedles (Figure 3A). However, the magnified view shown in Figure 3B clearly demonstrates that the nanotubes have irregular opened mouths with elliptical, forklike, and polygonal shapes. The nanotubes are 80–550 nm in diameter and over $10 \mu\text{m}$ in length, the thickness of the tube skin is only tens of nanometers. The XRD pattern of the nanotubes (not shown here) is similar to that of $\text{Cu}(\text{OH})_2$ nanoneedles. Parts C and D of Figure 3 are TEM images of the as-prepared $\text{Cu}(\text{OH})_2$ nanotubes. From Figure 3C, we realize that the nanotube seems to be formed by rolling a sheet. The SAED pattern of a 400 nm wide tube (inset of Figure 3D) demonstrates it is a single crystal, the tube is lying on its (010) plane, and the preferential growth direction

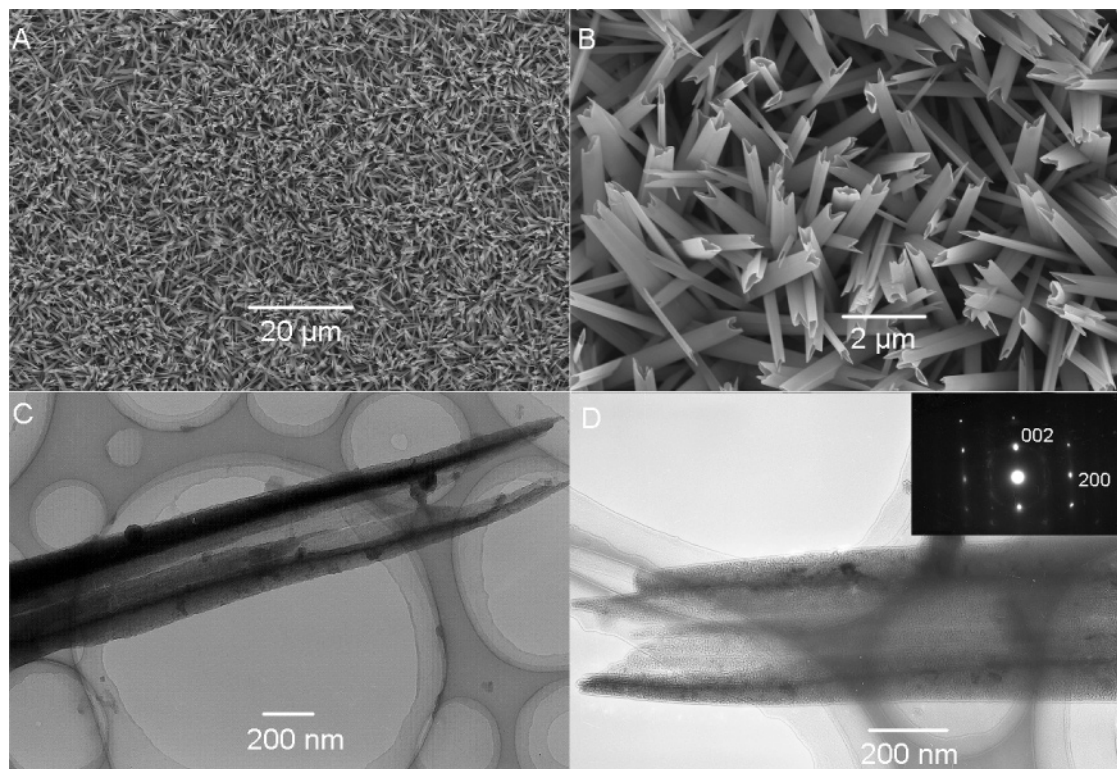


Figure 3. Typical SEM images of $\text{Cu}(\text{OH})_2$ nanotubes prepared at a constant current density of 1.5 mA cm^{-2} for 2.7 C cm^{-2} in 3.0 mol L^{-1} KOH solution at 28°C : (A) overall view; (B) a regional magnified view of A; (C, D) TEM images of the sample shown in B (insert, SAED).

of the single-crystal nanotube is its $[100]$ direction. Further increase of C_{KOH} to 3.5 mol L^{-1} will cause the dehydration of $\text{Cu}(\text{OH})_2$ to form CuO nanoparticles as listed in Table 1.

To understand the growth mechanism of $\text{Cu}(\text{OH})_2$ nanostructures, we have studied the effects of temperature and KOH concentration on the morphology of the nanostructures. Parts A–C of Figure 4 are the SEM images of $\text{Cu}(\text{OH})_2$ nanoneedles grown in 2.0 mol L^{-1} KOH solution at 1.5 mA cm^{-2} for 2.25 C cm^{-2} and at different temperatures. Comparing the nanoneedles grown at 2 or 15°C to those grown at 28°C , we can find that the number density of nanoneedles grown at a lower temperature is much higher than that formed at a higher temperature, and the nanoneedles trend to grow more upright (insert image of Figure 4C). Furthermore, as the temperature was decreased from 28 to 15 or 2°C , the average length of the nanoneedles decreased from 15 to about 10 or $5 \mu\text{m}$, correspondingly. The decrease of the nanoneedles' length is reflected in the increase of number density of the nanoneedles, because the total amounts of $\text{Cu}(\text{OH})_2$ on unit area are the same in these three cases. The higher number density implies that the nucleation of $\text{Cu}(\text{OH})_2$ crystals is easier at a lower temperature, so that more nanoneedles grow within the same time period. Parts D–F of Figure 4 show SEM images of a copper surface anodized in a 3.5 mol L^{-1} KOH solution at 1.5 mA cm^{-2} for 2.7 C cm^{-2} and at different temperatures. As shown in Figure 4D, at 28°C , only black CuO irregular nanoparticles were generated and covered the copper substrate compactly. These results indicate that a high KOH concentration and a high reaction temperature support the dehydration of $\text{Cu}(\text{OH})_2$ into CuO . However, it was interesting to find that $\text{Cu}(\text{OH})_2$ nanotubes were formed as the temperature was decreased to 15°C (Figure 4E). On further decrease of the temperature to 2°C , $\text{Cu}(\text{OH})_2$ nanoneedles were generated, instead of nanotubes (Figure 4F).

The influences of current density (I_d) on the resulting products have also been investigated. Figure 5 illustrates the SEM images and XRD patterns of the copper foil anodized in a 2 mol L^{-1} KOH aqueous solution at 28°C and at different current densities for 3 C cm^{-2} each. As shown in Figure 5A, in the case of $I_d = 0.5 \text{ mA cm}^{-2}$, black nanosheets or flowers (composed of staggered nanosheets) of CuO were generated, and they came along with a certain amount of Cu_2O (Figure 5D-a). This phenomenon indicated that the dehydration of $\text{Cu}(\text{OH})_2$ to CuO is a competition reaction to the growth of $\text{Cu}(\text{OH})_2$ nanocrystals at the nucleation process. At a low current density of 0.5 mA cm^{-2} , the amount of as-formed $\text{Cu}(\text{OH})_2$ was not sufficient for growing crystals. Thus, it tended to dehydrate into CuO for its high reaction activity. Cuprous oxide was generated by the competition oxidation of copper ($\text{Cu} + 2\text{OH}^- \rightarrow \text{Cu}_2\text{O} \downarrow + 2\text{e}^- + \text{H}_2\text{O}$) as described above. When I_d was increased up to over 1 mA cm^{-2} , $\text{Cu}(\text{OH})_2$ nanoneedles were produced instead of CuO (Figure 5B). Further increase of I_d , the number density of the nanoneedles, was increased due to the increase of nucleation rate, while the needle length was decreased (Figure 5C). Figure 5D shows XRD patterns of as-prepared products, the peaks marked with stars are diffraction lines of a copper substrate. As can be seen from Figure 5D-a, the wide diffraction peaks at 35.5° and 38.7° reveal that the resulting CuO is polycrystalline. The diffraction peaks at 29.6° (110), 36.4° (111), and 42.3° (200) can be indexed to cubic cuprous oxide (JCPDS 78-2076). The strong diffraction line at 61.5° is an overlapped peak of CuO (-113) and Cu_2O (220). The overall features of Figure 5D-b are similar to those of Figure 2A except that there are no diffraction peaks of Cu_2O . This results revealed that the increase of current intensity supports the formation of $\text{Cu}(\text{OH})_2$, and the side product, Cu_2O , can be effectively avoided. Figure 5D-c is similar to that of the $\text{Cu}(\text{OH})_2$ powder diffraction pattern, which is consistent with the SEM image shown in Figure 5C.

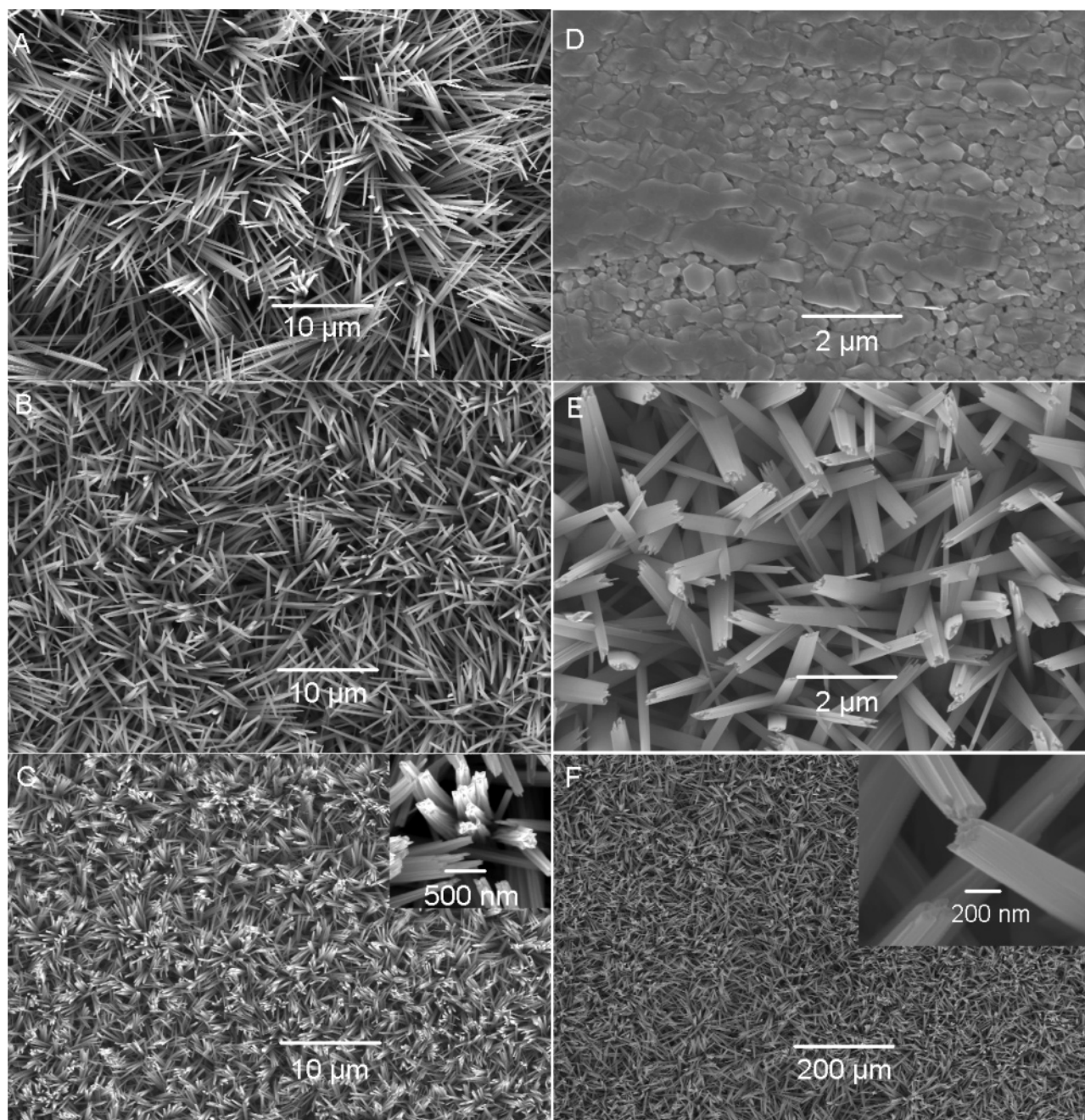
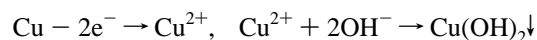


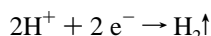
Figure 4. The surface morphology of a copper foil anodized in a 2 mol L⁻¹ (A–C) or 3.5 mol L⁻¹ (D–F) KOH solution at a constant current density of 1.5 mA cm⁻² for 2.25 C cm⁻² (A–C) or 2.7 C cm⁻² (D–F) and at different temperatures: (A) 28 ± 2 °C; (B) 15 ± 2 °C; (C) 2 ± 2 °C; (D) 28 ± 2 °C; (E) 15 ± 2 °C; (F) 2 ± 2 °C. Inserts show magnified views.

On the basis of the investigations described above, the formation mechanism of Cu(OH)₂ can be postulated as follows. The growth of pine-needle-like and scroll-like Cu(OH)₂ nanostructure arrays is an electrochemical process and can be simply represented by the following two electrochemical half reactions:

anode



cathode



Gas bubbles were observed to be released from the counter electrode surface during the electrolysis process, indicating the formation of H₂. The electrochemical reaction rate was con-

trolled mainly by current density. As the electrochemical reaction was carried out in a medium with a KOH concentration lower than 0.5 mol L⁻¹, no Cu(OH)₂ nanoneedle was produced. Gas bubbles were generated at both working and counter electrodes, and the whole electrochemical reaction is just the electrolysis of water. This is mainly because a compact Cu(OH)₂ film was initially formed on copper surface which prevented the substrate from further oxidation. The passivation film could not be formed as KOH concentration was increased to over 1 mol L⁻¹ and nanoneedles were obtainable. The main compete reaction to the growth of Cu(OH)₂ nanostructures is dehydration of Cu(OH)₂ to CuO. This is a chemical process and its reaction rate depends on the concentration of KOH and the reaction temperature, while depending little on current density. The Cu(OH)₂ formed in the initial stage of electrolysis is active in an alkaline solution.^{9–11,28} The increase of reaction

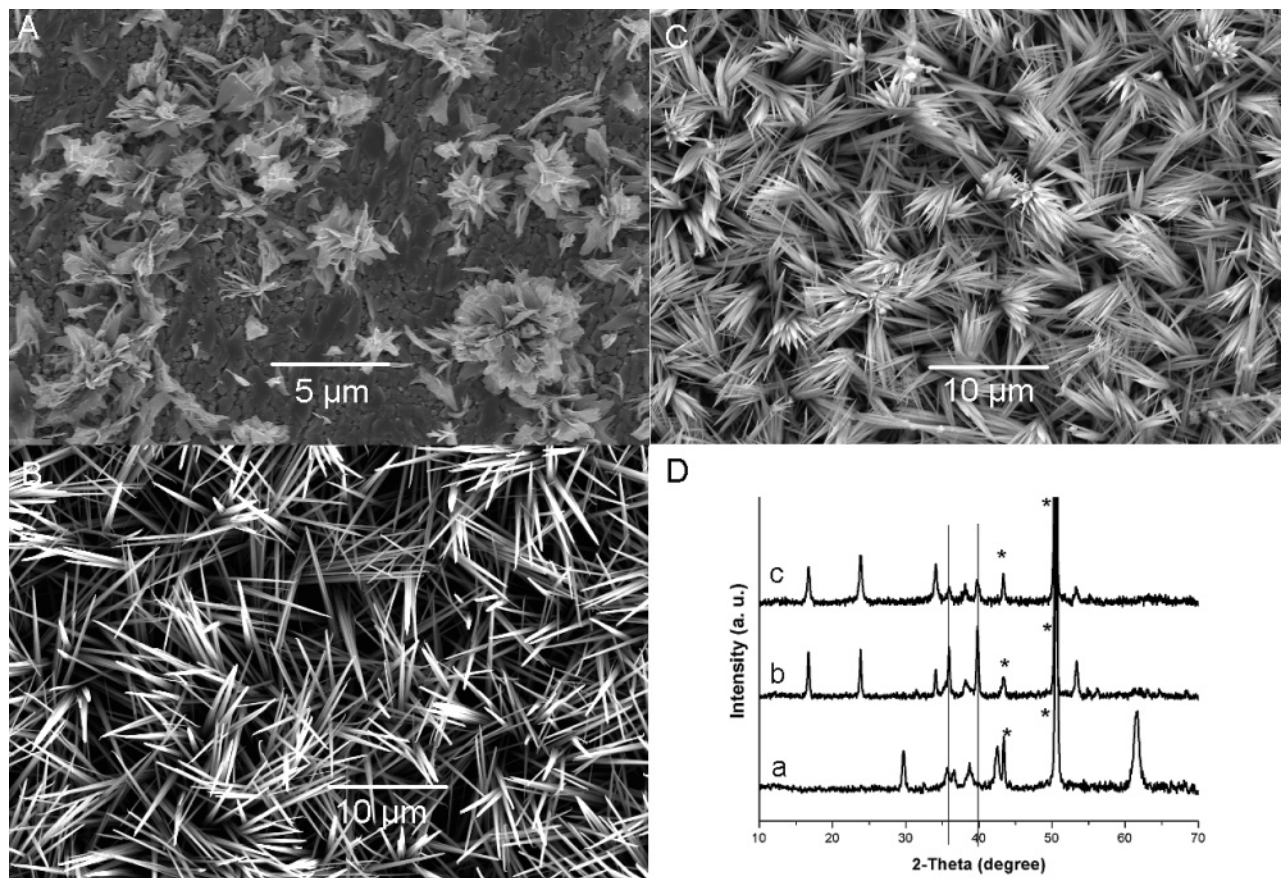


Figure 5. Typical SEM images (A–C) and XRD patterns (D) of a copper surface after anodizing in a 2.0 mol L^{-1} KOH solution at $28 \text{ }^\circ\text{C}$ and at different current densities for 3 C cm^{-2} each: (A) 0.5 mA cm^{-2} ; (B) 2 mA cm^{-2} ; (C) 6 mA cm^{-2} ; (D) XRD patterns at (a) 0.5 mA cm^{-2} ; (b) 2 mA cm^{-2} ; (c) 6 mA cm^{-2} .

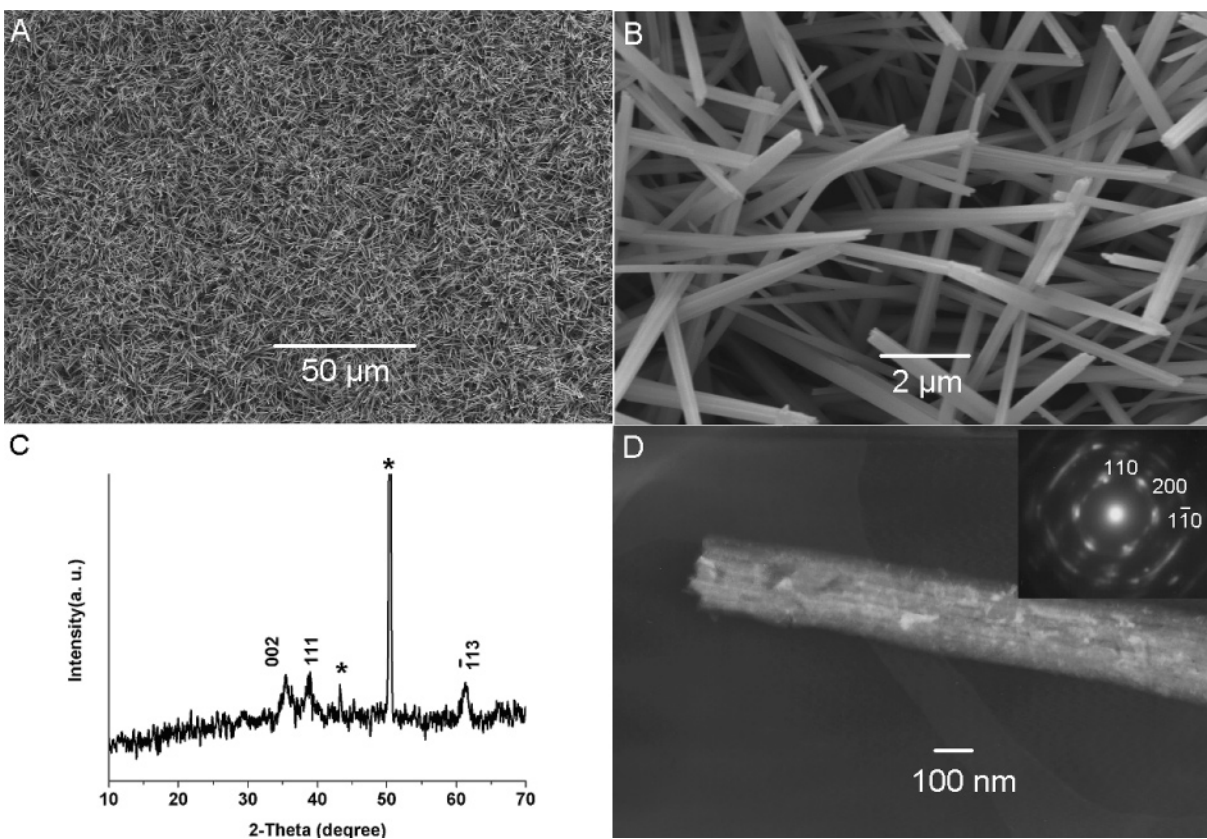


Figure 6. Typical SEM images (A, B), XRD pattern (C), and TEM image (D) of CuO nanoneedles converted from the as-prepared $\text{Cu}(\text{OH})_2$ nanoneedles: (A) overall view; (B) a magnified view; Insert of D: a SAED pattern.

temperature and KOH concentration accelerated the dehydration rate of $\text{Cu}(\text{OH})_2$, while the increase of current density increases the growth rate of $\text{Cu}(\text{OH})_2$ nanostructures. Thus, high temperature and high concentration of KOH and a low current density favor the formation of CuO nanoparticles film ($T > 28\text{ }^\circ\text{C}$, $C_{\text{KOH}} > 3.5\text{ mol L}^{-1}$ KOH, see Figure S2). The appropriate conditions for the $\text{Cu}(\text{OH})_2$ nanoneedles and nanotubes are summarized in Table 1. Accordingly, nanoneedles are formed in the systems with lower KOH concentrations and at lower temperatures than those used for growing nanotubes.

It is known that different growth rates of the crystal faces determine the ultimate morphology of the nanomaterial.¹⁵ The growth of $\text{Cu}(\text{OH})_2$ nanoneedles along the [100] direction can be understood on the basis of the assembly of oblated chains $>\text{Cu}(\text{OH})_2\text{Cu}<$ in the plane (001), oriented along [100].^{9–11,27} According to the Bravais–Friedel–Donnay–Harker law,^{29,30} the growth rate of orthorhombic $\text{Cu}(\text{OH})_2$ crystal is normally proportional to $1/d_{hkl}$. So the growth of $\text{Cu}(\text{OH})_2$ along [100] is much faster than those along the other directions, leading to the formation of ribbonlike nanostructures. The nanoneedle was formed by stacking the nanoribbons with hydrogen bonding interactions. In a solution with high KOH concentration or at high reaction temperature, the interlayer hydrogen bond linkages at the sheet edges were weakened, which caused stresses in the layers. So, the ribbons were rolled to relieve the stresses, forming the final scroll-like tubular structure.^{13,16,30}

Dehydration of $\text{Cu}(\text{OH})_2$ nanoneedles at $150\text{ }^\circ\text{C}$ for 3 h and then further crystallized at $200\text{ }^\circ\text{C}$ for another 3 h produced CuO nanoneedles. As can be seen from Figure 6A,B, the CuO nanoneedles preserved the morphology of the $\text{Cu}(\text{OH})_2$ precursors. The XRD pattern of as-prepared CuO nanoneedles (Figure 6C) reveals that the conversion of $\text{Cu}(\text{OH})_2$ to monoclinic CuO is complete. The weak peaks of the XRD pattern indicate that CuO nanoneedles are polycrystalline (the peaks marked with stars are attributed to copper foil). Figure 6D is the TEM images of a single CuO nanoneedle, the SAED image in the insert reveals that the CuO nanoneedle was lying on the (001) plane and axis direction is along $[-110]$, which is consistent with the result reported in the literature.^{13,17,30}

Conclusions

In summary, large area $\text{Cu}(\text{OH})_2$ nanoneedle and nanotube arrays can be fabricated by simply anodization of a copper foil in an aqueous solution of KOH without any template and additive. The nanostructures are made of $\text{Cu}(\text{OH})_2$ nanosheets. The advantages of our method for preparation of these inorganic nanostructures lie in its simplicity, mild reaction conditions and by the ability to control the lengths, number densities, and shapes (needle or tube) of the nanostructures to some extent through modulation the experimental parameters including temperature, concentration of KOH, and current density. The optimum conditions for producing $\text{Cu}(\text{OH})_2$ nanoneedles or nanotubes

are summarized in Table 1. Furthermore, CuO nanoneedles, a novel nanomaterial with various potential applications, can be simply produced by heating their $\text{Cu}(\text{OH})_2$ precursors.

Acknowledgment. This work was supported by National Natural Science Foundation of China (90401011, 20374034, 50225311) and 973 project (2003CB615700).

Supporting Information Available: TEM images of $\text{Cu}(\text{OH})_2$ nanoneedles and CuO film. This material is available free of charge via the Internet at <http://pubs.acs.org>.

References and Notes

- (1) Cui, Y.; Wei, Q. Q.; Park, H. K.; Lieber, C. M. *Science* **2001**, *293*, 1289.
- (2) Martin, C. R. *Science* **1994**, *266*, 1961.
- (3) Hulstee, J. C.; Martin, C. R. *J. Mater. Chem.* **1997**, *7*, 1075. Sapp, S. A.; Lakshmi, B. B.; Martin, C. R. *Adv. Mater.* **1999**, *11*, 402.
- (4) Dingman, S. D.; Rath, N. P.; Markowitz, P. D.; Gibbons, P. C.; Buhro, W. E. *Angew. Chem., Int. Ed.* **2000**, *39*, 1470.
- (5) Pan, Z. W.; Dai, Z. R.; Ma, C.; Wang, Z. L. *J. Am. Chem. Soc.* **2002**, *124*, 1817.
- (6) Liu, R.; Vertegel, A. A.; Bohannan, E. W.; Sorenson, T. A.; Switzer, J. A. *Chem. Mater.* **2001**, *13*, 508.
- (7) Ren, Z. F.; Huang, Z. P.; Xu, J. W.; Wang, J. H.; Bush, P.; Siegal, M. P.; Provencio, P. N. *Science* **1998**, *282*, 1105.
- (8) Nigro, R. L.; Malandrino, G.; Fraga, I. L. *Chem. Mater.* **2001**, *13*, 4402.
- (9) Kratochvil, S.; Matijević, E. *J. Mater. Res.* **1991**, *6*, 766.
- (10) Rodríguez-Clemente, R.; Serna, C. J.; Ocaña, M.; Matijević, E. *J. Cryst. Growth* **1994**, *143*, 277.
- (11) Lee, S. H.; Her, Y. S.; Matijević, E. *J. Colloid Interface Sci.* **1997**, *186*, 193.
- (12) Du, G. H.; Van Tendeloo, G. *Chem. Phys. Lett.* **2004**, *393*, 64.
- (13) Lu, C. H.; Qi, L. M.; Yang, J. H.; Zhang, D. Y.; Wu, N. Z.; Ma, J. M. *J. Phys. Chem. B* **2004**, *108*, 17825.
- (14) Song, X. Y.; Sun, S. X.; Zhang, W. M.; Yu, H. Y.; Fan, W. L. *J. Phys. Chem. B* **2004**, *108*, 5200.
- (15) Wen, X. G.; Zhang, W. X.; Yang, S. H.; Dai, Z. R.; Wang, Z. L. *Nano Lett.* **2002**, *2*, 1397.
- (16) Zhang, W. X.; Wen, X. G.; Yang, S. H.; Berta, Y.; Wang, Z. L. *Adv. Mater.* **2003**, *15*, 822.
- (17) Wen, X. G.; Zhang, W. X.; Yang, S. H. *Langmuir* **2003**, *19*, 5898.
- (18) Park, S. H.; Kim, H. J. *J. Am. Chem. Soc.* **2004**, *126*, 14368.
- (19) Diggle, J. W.; Downie, T. C.; Goulding, C. W. *Chem. Rev.* **1969**, *69*, 365.
- (20) Macák, J. M.; Tsuchiya, H.; Schmuki, P. *Angew. Chem., Int. Ed.* **2005**, *44*, 2100.
- (21) Zhang, J. X.; Shi, G. Q.; Liu, C.; Qu, L. T.; Fu, M. X.; Chen, F. E. *J. Mater. Sci.* **2003**, *38*, 2423.
- (22) Pan, H.; Liu, B. H.; Yi, J. B.; Poh, C.; Lim, S.; Ding, J.; Feng, Y. P.; Huan, C. H. A.; Lin, J. Y. *J. Phys. Chem. B* **2005**, *109*, 3094.
- (23) MacDonald, A. H. *Nature* **2001**, *414*, 409.
- (24) Macilwain, C. *Nature* **2000**, *403*, 121.
- (25) He, H.; Bourges, P.; Sidis, Y.; Ulrich, C.; Regnault, L. P.; Pailhes, S.; Berzigiarova, N. S.; Kolesnikov, N. N.; Keimer, B. *Science* **2002**, *295*, 1045.
- (26) Reitz, J. B.; Solomon, E. I. *J. Am. Chem. Soc.* **1998**, *120*, 11467.
- (27) Oswald, H. R.; Reller, A.; Schmalle, H. W.; Dubler, E. *Acta Crystallogr., Sect. C* **1990**, *46*, 2279.
- (28) Cudennec, Y.; Lecerf, A. *Solid State Sci.* **2003**, *5*, 1471.
- (29) Hartman, P.; Perdok, W. G. *Acta Crystallogr.* **1955**, *8*, 49.
- (30) Zhang, W. X.; Wen, X. G.; Yang, S. H. *Inorg. Chem.* **2003**, *42*, 5005.